Kufa Journal of Engineering
Vol. 15, No. 2, April 2024, P.P. 39-60
Article history: Received 7 August 2023, last revised 20 January 2024, accepted 1 February 2024

GRAPHITE FOAM STRUCTURES AS AN EFFECTIVE MEANS TO COOL HIGH-PERFORMANCE ELECTRONICS

Ahmed Alhusseny [1], Qahtan Al-Aabidy [2], Nabeel Al-Zurfi [3],

Adel Nasser [4], Mohammed Al-Edhari [5], and Hayder Al-Sarraf [6]

[1] Asst. Prof., Department of Mechanical Engineering, Faculty of Engineering, University of Kufa, Al-Najaf, Iraq, Email: ahmedn.alusseini@uokufa.edu.iq; Visiting Researcher, Department of Mechanical, Aerospace and Civil Engineering, University of Manchester, Manchester, UK. Email: ahmed.alhusseny@manchester.ac.uk

[2] Asst. Prof., Department of Mechanical Engineering, Faculty of Engineering, University of Kufa, Al-Najaf, Iraq, Email: qahtan.alaabidy@uokufa.edu.iq; Visiting Researcher, Department of Mechanical, Aerospace and Civil Engineering, University of Manchester, Manchester, UK. Email: qahtan.alaabidy@manchester.ac.uk

[3] Asst. Prof., Department of Mechanical Engineering, Faculty of Engineering, University of Kufa, Al-Najaf, Iraq, Email: nabeelm.alzurfi@uokufa.edu.iq; Visiting Researcher, Department of Mechanical, Aerospace and Civil Engineering, University of Manchester, Manchester, UK. Email: nabeel.al-zurfi@manchester.ac.uk

[4] Senior Lecturer, Department of Mechanical, Aerospace and Civil Engineering, University of Manchester, Manchester, UK, Email: a.g.nasser@manchester.ac.uk

[5] Assistant Lecturer, Department of Mechanical Engineering, Faculty of Engineering, University of Kufa, Al-Najaf, Iraq. Email: mohammedf.jaber@uokufa.edu.iq

[6] PhD Student, Department of Mechanical Engineering, Design & Creative Technologies, Auckland University of Technology, Auckland, New Zealand. Email: hayder.al-sarraf@autuni.ac.nz

https://doi.org/10.30572/2018/kje/150204

ABSTRACT

Due to their unique heat transfer features, graphite foams are used in the current analysis to form heat sinks effective enough to dissipate extreme heat generated within high-performance electronics. The heat sinks proposed are formed from foamed-baffles arranged either in parallel or perpendicular to the coolant paths through the staggered slots in between to alleviate the penalty of pressure drop while maintaining high heat dissipation capability. Two different sorts of dielectric coolants namely, air and the FC-3283 electronic liquid developed by 3M^{TM}, have

been utilized to directly dissipate the heat generated. The feasibility of the currently proposed heat sinks has been examined numerically based on the volume averaging concept of porous media employing the local thermal non-equilibrium model to account for interstitial heat exchange between the foam solid matrix and the fluid particles flowing across. A wide range of design parameters has been tested including the heat sink configuration along with structural characteristics of the graphite foam used. It has been found that foam baffles oriented perpendicular to the path of coolant flow can dissipate heat by about 50% better than those parallel to it, but with higher pressure losses. It has also been found that heat dissipation capability, for a certain orientation of baffles, can be improved by up to 100% when the foam pore size is doubled with outstanding saving in pressure losses by up to 300%. The impact of operating conditions, including the coolant flowrate and the heat flux applied, has also been inspected. The currently proposed heat sinks have been found efficient to meet the thermal demands of high-performance electronics and sweep away the extreme heat generated there with reasonable cost of pressure drop, where the proper selection of design parameters in light of the operating conditions applied can prevent the emergence of hot spots entirely. Extreme operating conditions, i.e. with heat density of up to 10W/cm^2 for air-cooled heat sinks and 100W/cm^2 for those cooled with FC-3283, can be well managed when a heat sink is configured from baffles that are oriented perpendicularly to the coolant flow path and formed of graphite foam having low porosity ($\emptyset = 0.8$) and larger pore size ($D = 800\mu m$).

KEYWORDS: Direct Electronics cooling, Heat sink, Porous, Graphite foam, Thermohydraulic performance.

1. INTRODUCTION

With the noticeably accelerated development in the microelectronic industry and telecommunication technology, electronic components used in such devices have become of higher performance, lighter weight, and more miniaturized. Nowadays, high-power electronic chips are being fabricated in a limited space available for heat dissipation, which results in a high heat density within electronic components. Accordingly, the reliability and safety of such devices will be jeopardized if the heat generated within them is not properly controlled. Therefore, thermal control has become of increasing importance while designing and operating electronic equipment, where it has become crucial to innovate more-effective methods capable to cool high-performance electronic chips. The key factors desired to fulfil in the applications of thermal management are high thermal conductivity, high compactness, low weight, and reasonable pressure loss. Such unique hydrothermal features are already in the DNA of either open-core foams formed from highly conductive materials such as metal- or graphite foams (Alhusseny, Al-Fatlawi, et al., 2021). Open-cell metal foams have, for instance, been successfully employed in diversity of thermal applications including heat exchangers (Alhusseny, Turan and Nasser, 2017), latent heat thermal energy storage units (Alhusseny et al., 2020), and the cooling of turbine blades (Al-Aabidy, Alhusseny and Al-Zurfi, 2021) as well as electrical generators (Alhusseny et al., 2015). On the other hand, the ORNL graphite foams (Klett et al., 2000) that predominantly possess spherical pores have the potentials to fulfil most of the above-mentioned requirements desirable in thermal management applications (Alhusseny, Al-Aabidy, et al., 2021). The thermal conductivity of graphite foam ligaments can be up to 1900 W/m·K resulting in effective thermal conductivity as high as 180 W/m·K or more, which is comparable to the dense aluminium and 80% lighter, not to mention the very large surface area available for heat exchange within a given volume of the foam, i.e. 5000–50,000 m2/m3 (Straatman, 2011). Due to their promising thermal properties, many researchers have adopted graphite foams as an effective medium for thermal management applications. To name a few, they have been utilized successfully in radiator systems for vehicles (Klett, Ott and McMillan, 2000), natural gas powered heat pumps (Ott, Zaltash and Klett, 2002), compact recuperators (Straatman et al., 2007) with superior effectiveness of 98% (Wu et al., 2009), corrosionless heat exchangers used in heat recovery from the exhaust gases of fossil-fuel powered power plants (Thompson, 2014), thermal control of electronic elements (Qu et al., 2024), and many more (Lin, Yuan and Sunden, 2011).

Due to the very small openings between the foam cells, the graphite foam solid matrix exhibits, however, too high resistance to fluid flow across it, which in turn may cause extreme pressure losses. Thus, increasing attention has been paid during the design of thermal systems based on graphite foams to reduce the pressure losses while keeping the heat transfer performance at desired levels. In this context, a variety of graphite foam configurations, e.g. (Gallego and Klett, 2003), have been proposed and examined in light of the overall performance achieved for electronics cooling, where it was pointed out that appropriate configuration of graphite foams can present a promising heat sink capable to dissipate the heat demanded with relatively low pressure drop. Similar findings have been found regarding the use of corrugated carbon foam blocks for recuperators (Lin et al., 2010) as well as the heat exchangers formed of baffle, pined, corrugated and wavy corrugated graphite foam fins for vehicles applications (Lin, Sundén and Yuan, 2013), where the thermal performance acquired was improved through introducing proper design of graphite foam configurations.

Motivated by thermal advantages of graphite foams and bearing in mind the high pressure drop expected due to them, innovative heat sinks to cool high-performance electronic equipment are proposed. The configurations suggested have the potentials to dissipate excessive thermal loads with affordable pressure drop, which to the authors' knowledge have not been addressed before.

2. MATHEMATICAL MODELLING

2.1. Problem description

The overall size of the graphite foam heat sink proposed is $L_s \times W_s \times H_s = (60mm \times 60mm \times 30mm)$ and formed of $\{L_b(mm)long \times W_b(mm)thick \times H_b(mm)high\}$ staggered baffles extended over a base of height $H_{base} = 5mm$ that is fixed on the heated surface. The foam baffles are arranged either perpendicularly or in-parallel to the coolant flow direction, as illustrated in Fig. 1, where five heat sinks of different number of foam baffles have been configured with different dimensions according to their length-to-width ratio as detailed in Table 1. The coolant flow domain has further been extended $20mm$ upstream and $120mm$ downstream from the heat sink.

Table 1. Dimensions of foam baffles and clear voids enclosed.

A_b	Number of Baffle	$L_b = L_v$ (mm)	$W_b = W_v$ (mm)
0.2	90	2	10
0.4	180	2	5
1	450	2	2
2.5	180	5	2
5	90	10	2

The heat and fluid flow domain to be examined is composed of two physically different regions, i.e. cooling fluid and graphite foam heat sink. The graphite foam used is assumed to be rigid, homogeneous, and isotropic with graphite thermal conductivity of 1900W m^{-1} K^{-1}, where three pore sizes (400,600, 800) μm along with three porosities (0.8, 0.85, 0.9) have been considered, which cover the area of interest for most of heat transfer applications (DeGroot and Straatman, 2012). The pore geometry of the graphite foam considered has been modelled based on the spherical void phase (SVP) idealised by (Yu, Thompson and Straatman, 2006), as shown in Fig. 2. In this model, the dimension of the unit-cube H is characterized in terms of the pore diameter D and the foam porosity $\emptyset$ as follows:

$$H^3 - \frac{3\pi D^2 H}{4\emptyset+\pi} + \frac{4\pi D^3}{3(4\emptyset+\pi)} = 0 \quad (1)$$

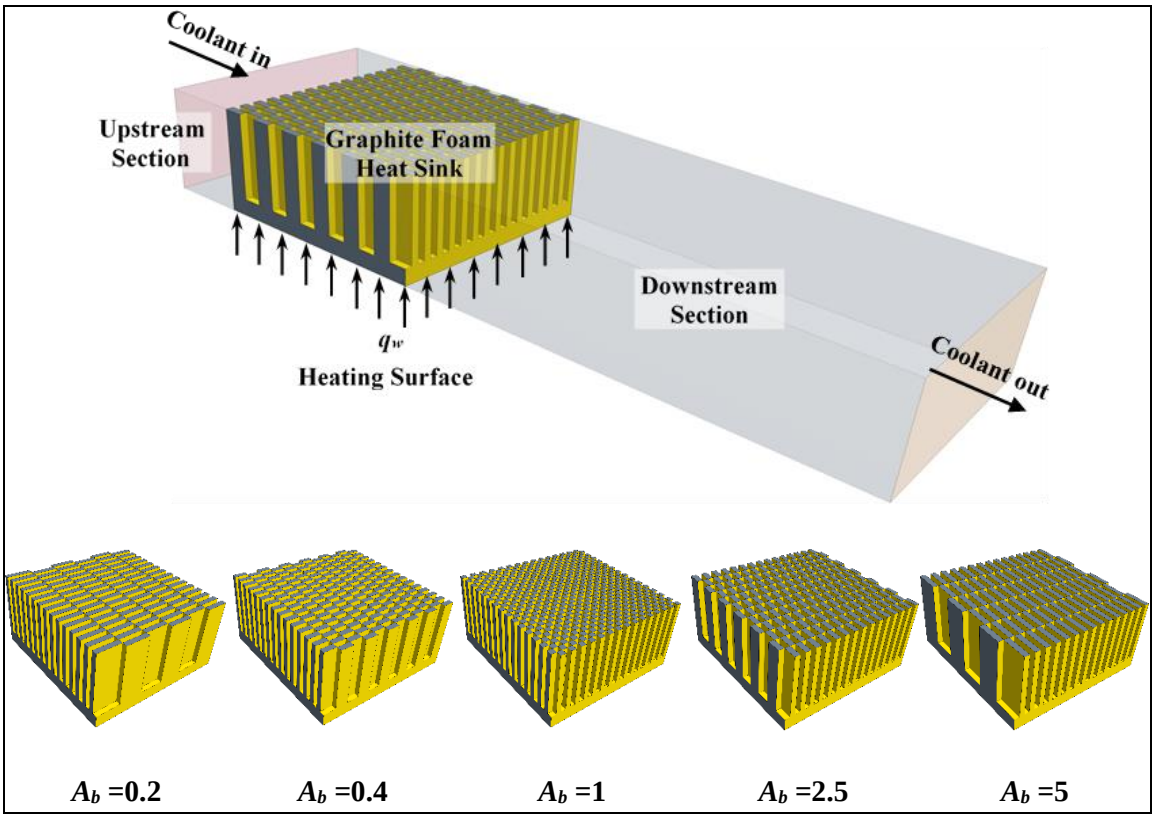

Fig. 1. Description of the problem examined: flow domain (up), heat sink configuration (down).

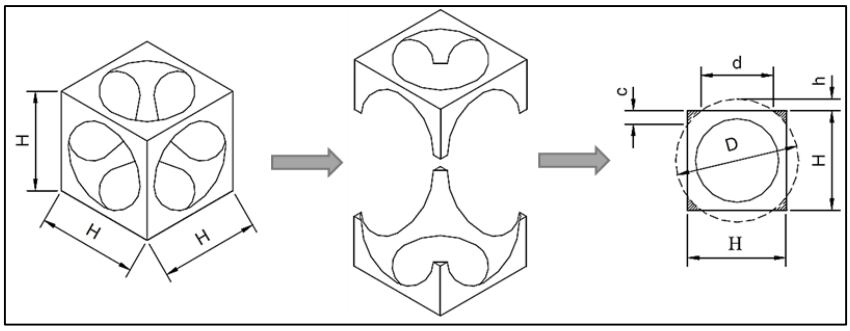

Fig. 2. Detailed dimensions of the unit cube model (Yu, Thompson and Straatman, 2006)**.**

2.2. Assumptions and governing equations

Two sorts of dielectric coolants have been used according to the level of heat density to be dissipated. For relatively low heat densities ($q_{\mathrm{w}} \in (1, 10)\, W/cm^2$), the coolant used is air; while the FC-3283 electronic liquid developed by 3M™ (3M$^{\mathrm{TM}}$, 2019) is used to meet thermal demands for extremer operating conditions, i.e. $q_{\mathrm{w}} \in (10, 100)\, W/cm^2$. Due to the excessive thermal densities generated in the high-performance electronics to be examined, thermo-physical properties of the coolants used are considered temperature-dependent to accord with the wide range expected for fluid-temperatures. Therefore, air has been treated as ideal gas and its dynamic viscosity and thermal conductivity have been estimated according to the Sutherland's law, while the temperature-dependent properties of FC-3283 liquid are computed according to the product data given by the manufacturer (3M$^{\mathrm{TM}}$, 2019). The coolant flow through the foam structures is assumed steady, incompressible, and laminar, where the pore-Reynolds number considered has been limited to $Re_{D_{in}} \leq 100$ in order to avoid the onset of transient and/or turbulent effects (DeGroot and Straatman, 2012). Following the volume-averaging approach and taking into account the local thermal non-equilibrium between the solid and fluid constituents in the representative elemental volume, the conservation equations governing the transport of mass, momentum, fluid-phase, and solid-phase energy are as follows:

$$\nabla \cdot (\rho_{\mathrm{f}} \mathbf{v}) = 0 \tag{2}$$

$$\emptyset^{-2} \nabla \cdot (\rho_{\mathrm{f}} u_{\mathrm{i}} \mathbf{v}) = -\nabla p + \emptyset^{-1} \mu \nabla^2 u_{\mathrm{i}} - \gamma \left(\mu K^{-1} + \rho_{\mathrm{f}} c_{\mathrm{F}} K^{-1/2} |\mathbf{v}| \right) u_{\mathrm{i}} \tag{3}$$

$$\rho_{\mathrm{f}} c_p (\mathbf{v} \cdot \nabla) T_{\mathrm{f}} = (1 - \gamma) k_{\mathrm{f}} \nabla^2 T_{\mathrm{f}} + \gamma [(k_{\mathrm{fe}} + k_{\mathrm{d}}) \nabla^2 T_{\mathrm{f}} + a_{\mathrm{sf}} h_{\mathrm{sf}} (T_{\mathrm{s}} - T_{\mathrm{f}})] \tag{4}$$

$$0 = k_{\mathrm{se}} \nabla^2 T_{\mathrm{s}} + a_{\mathrm{sf}} h_{\mathrm{sf}} (T_{\mathrm{f}} - T_{\mathrm{s}}) \tag{5}$$

Depending on the parameter γ and porosity $\emptyset$, only a particular set of the above compact equations is assigned to the relevant zone. In the porous zones, the values of γ and $\emptyset$ are respectively set to 1 and graphite foam porosity. Otherwise, they are respectively set to zero

and 1 in the non-porous zones. The foam permeability K and inertial coefficient c_F have been, on the other hand, computed using the data estimated during the pore-level calculations carried out by (DeGroot and Straatman, 2012). The effective thermal conductivities of the fluid- k_{fe} and solid-phase k_{se} as well as the specific interstitial heat transfer area a_{sf} have been estimated using the unit cube-based model by (Yu, Thompson and Straatman, 2006) developed for SVP graphite foams, while the dispersive thermal conductivity k_{d} and the interstitial heat transfer coefficient h_{sf} have been locally computed following the models developed in the above-mentioned pore-level simulations (DeGroot and Straatman, 2012).

Each coolant used is considered to have a uniform velocity and temperature at the inlet to the flow domain, i.e. $u_{in} = \mu Re_{D_{in}}/\left(\rho_{\mathrm{f}_{in}} D\right)$ & $T_{in} = 25℃$, while specified pressure condition is assumed at the outlet boundary. The baseplate represents the heating surface and is exposed to a uniform heat density q_{w} ranged respectively from 1 to 10 W/cm^2 and 10 to 100 W/cm^2 for air- and FC-3283-cooled heat sinks. Lastly, the equations that govern the fluid flow and heat transfer within each of the clear and porous zones need to be linked together at the interface surfaces separating them. Therefore, and to guarantee the continuity in each of the velocity, shear stress, fluid-temperature, and heat flux across the solid–fluid interface; the coupling conditions developed for that purpose (Ochoa-Tapia and Whitaker, 1997) have been adopted.

3. NUMERICAL METHOD

3.1. Grid generation and discretisation method

The physical domain of the problem considered has been meshed using hexahedral elements to form an entirely structured grid everywhere in the problem domain, as shown in Fig. 3. Attention has been paid while structuring the solution grid to keep the interfaces (between the physically different regions) conformal everywhere. Also, more grid points have been clustered close to the baseplate as well as clear-porous interface surfaces in order to capture the steep gradients expected there.

The finite volume method has been adopted to discretise the governing equations with employing the SIMPLE algorithm to resolve the problem of velocity–pressure coupling. The heat and fluid flow has been solved iteratively using the "Simcenter STAR-CCM+" commercial CFD software. The second-order upwind scheme has been adopted to implement spatial discretisation of momentum and energy. To overcome convergence difficulties, the iterative solution of each of the velocity components, pressure-correction, fluid-phase and solid-phase temperature has been under-relaxed with a factor equal to 0.7, 0.3, 0.9, 0.99, respectively.

Solution convergence has been checked in terms of the change in each variable at the end of each iteration, where the maximum residual allowed in each of the continuity, momentum, and energy equations is 10-6. When this criterion is fulfilled, the final solution is attained, where the data computed are post-processed to explore the feasibility of the heat sinks proposed.

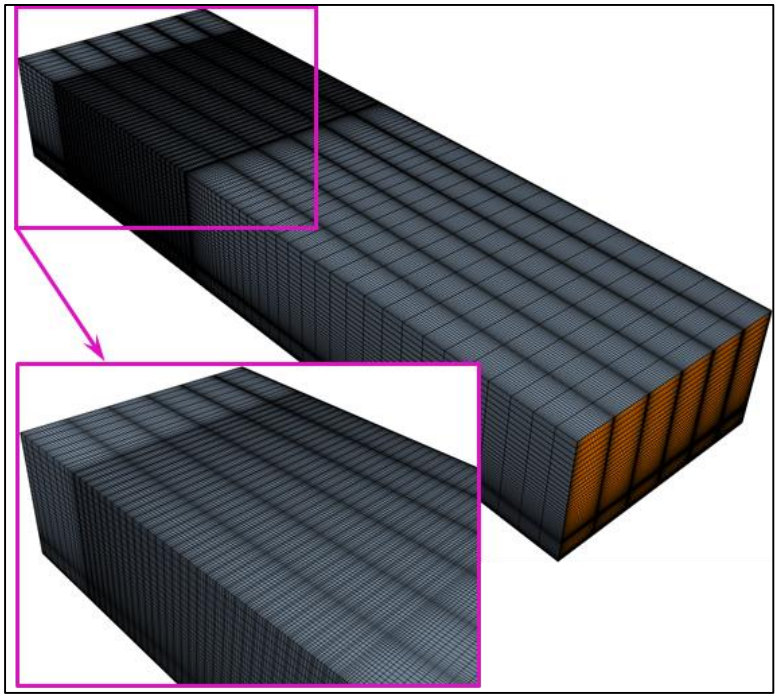

Fig. 3. The mesh used for the $A_b = 0.2$ foam heat sink.

3.2. Validation of the numerical procedure

The validity of the mathematical modelling adopted along with the numerical procedures utilized has been checked by comparing the currently computed data with the experimental data reported by (Leong et al., 2010), as shown in Figs. 4 & 5. It is obvious that the data computed numerically agree fairly well with the data recorded experimentally. Thus, the reliability of the methodology followed along with the computational approaches adopted has been confirmed, and apparently there is no concern from using the current computational program to track fluid flow and heat transfer accurately in the current investigation.

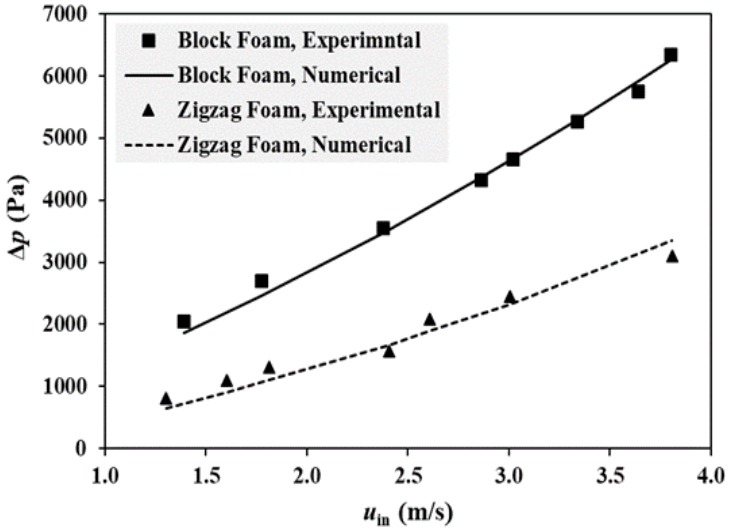

Fig. 4. Validation of computed pressure drop.

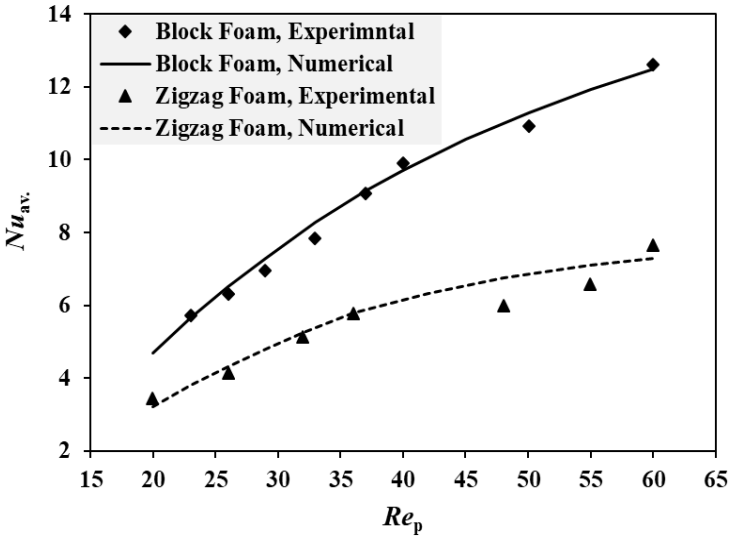

Fig. 5. Validation of computed Nusselt number.

4. RESULTS

Computations are carried out for a wide range of design and operating parameters of the graphite foam heat sinks proposed. The design parameters including the baffle length-to-width ratio, foam porosity, and pore size, are respectively ranged as $A_b \in (0.2\sim5)$, $\emptyset \in (0.8\sim0.9)$, $D \in (400\sim 800)\mu m$. The operating conditions, on the other hand, including the inlet pore-Reynolds number and heat flux are ranged as $Re_{D_{in}} \in (20\sim100)$ and $q_{\mathrm{w}} \in (1\sim100)\, W/cm^2$ depending on the sort of coolant utilized. The results obtained are presented in terms of Nusselt number, pressure drop, foam mass flowrate fraction, temperature rise, and thermal performance factor.

4.1. Impact of heat sink configuration

The influence of heat sink configuration can be summarized in Figs. 6 & 7 regarding the average Nusselt number, dimensionless pressure drop, and the fraction of mass flowrate across the foam structures for air-cooled and FC-3283-cooled heat sinks subjected to heat density of 5 and $50\,W/cm^2$, respectively. It can be seen that the heat transfer performance is, in general, downgraded with the increase in the baffle length-to-width ratio (A_b). However, such a reduction in heat transfer performance is accompanied by a valuable advantage, which is the significant saving achieved in pressure drop. Such conflicting outcomes can be justified by having a close look at the penetration extent of coolant into the porous structures. This is done by monitoring the fraction of coolant mass penetrating the foam ($\dot{m}_{\text{foam}}/\dot{m}_{\text{total}}$), which represents the ratio of the coolant mass flow rate penetrating through foam structures to the total mass flow rate of the coolant. When baffles orientation changes from being in line with the direction of coolant mainstream ($A_b > 1$) to perpendicular to it ($A_b < 1$), more amount of coolant will penetrate the porous baffles carrying more heat away from the foam matrix, which in turn improves the cooling effectiveness considerably. As further amount of coolant flows via the foam pores, further pumping energy is, however, consumed to cope with the inevitable boost in pressure loss as a result of accelerating the coolant particles passing across the foam baffles.

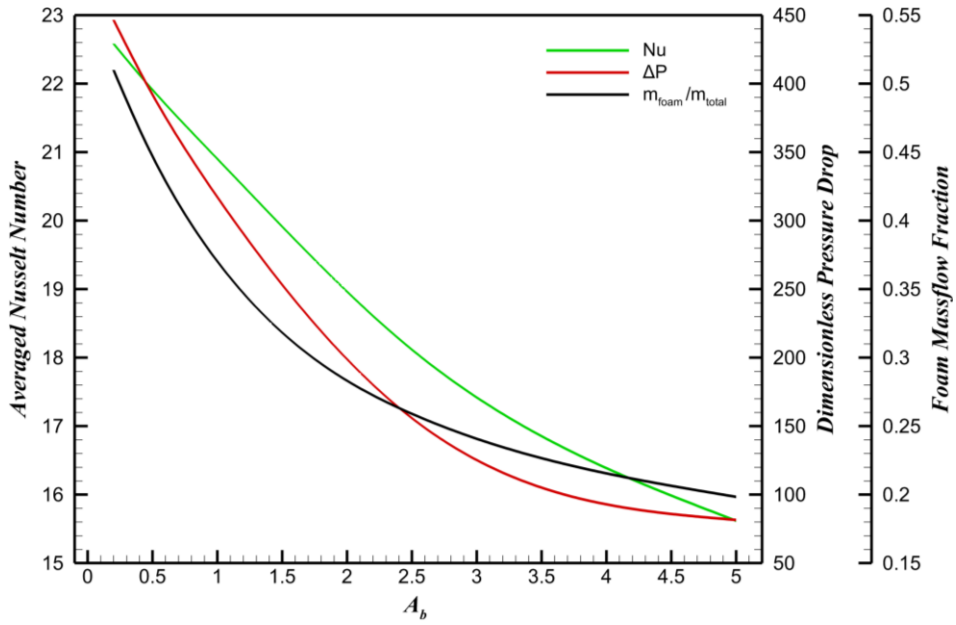

Fig. 6. Nusselt number, dimensionless pressure drop, and foam mass flowrate fraction for air-cooled heat sinks with $Re_{D_{in}} = 100$, $\emptyset = 0.8$ & $D = 400\mu m$.

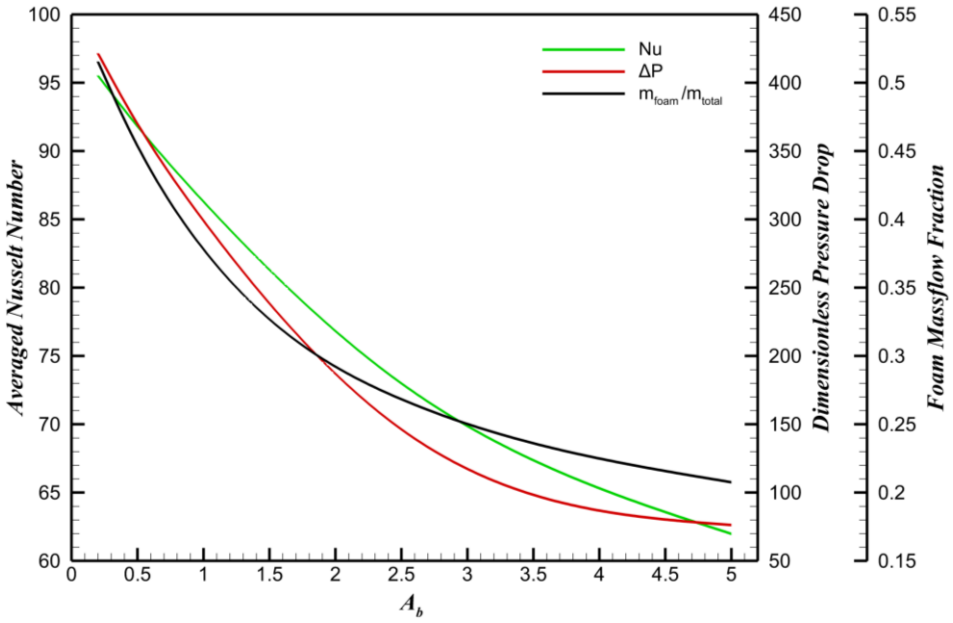

Fig. 7. Nusselt number, dimensionless pressure drop, and foam mass flowrate fraction for FC-3283-cooled heat sinks with $Re_{D_{in}} = 100$, $\emptyset = 0.8$ & $D = 400\mu m$.

4.2. Influence of foam structural characteristics

Graphite foam pore-structure is mainly characterized by two geometrical parameters, namely the porosity $\emptyset$ and pore diameter D. Hence, it is essential to explore the effects of those design parameters on the performance achieved. Combined effects of changing the pore diameter and baffles aspect ratio on the performance obtained are summarized in Figs. 8 & 9 concerning the mean Nusselt number as well as pressure loss for air-cooled and FC-3283-cooled heat sinks, respectively. The pore-Reynolds number appointed to account for the flow condition at the inlet boundary is, however, not unified as the various sizes of pore diameter results in different values of coolant velocity at the inlet boundary, i.e. $u_{in} = \mu Re_{D_{in}}/(\rho_{f_{in}} D)$. Instead, a range of pore-Reynolds number has been considered such that a unified flow condition is adopted at the inlet for all the pore diameters tested, where for pore sizes of $D = (400, 600, 800)\ \mu m$, the pore-Reynolds number examined are respectively $Re_{D_{in}} = (50, 75, 100)$. At first glance, it is anticipated that heat sinks with larger pore sizes offer less effective cooling because the specific surface area available for solid–fluid interfacial heat exchange decreases with the increase of foam pore diameter. However, this is not the case found in Figs. 8 & 9, where it is apparent that heat sinks fabricated of foam with larger pores are capable to dissipate heat more effectively. This might be attributed to the simultaneous increase attained in the penetration of coolant into the foam matrix. While increasing the size of foam pores, the porous matrix becomes more permeable, and hence, less resistant to the coolant particles flowing across. Accordingly, more

fluid particles can be induced to flow inside the foam, which in turn makes up the degrade resulting in heat transfer due to the reduction in the interstitial heat transfer area.

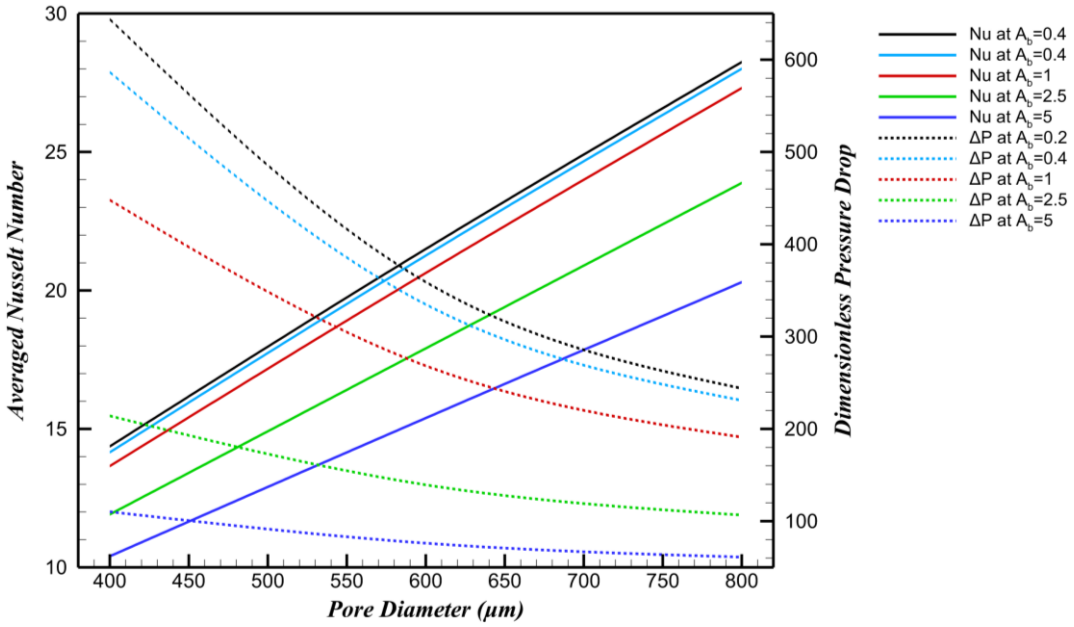

Fig. 8. Impact of pore size and baffles arrangement for air-cooled heat sinks.

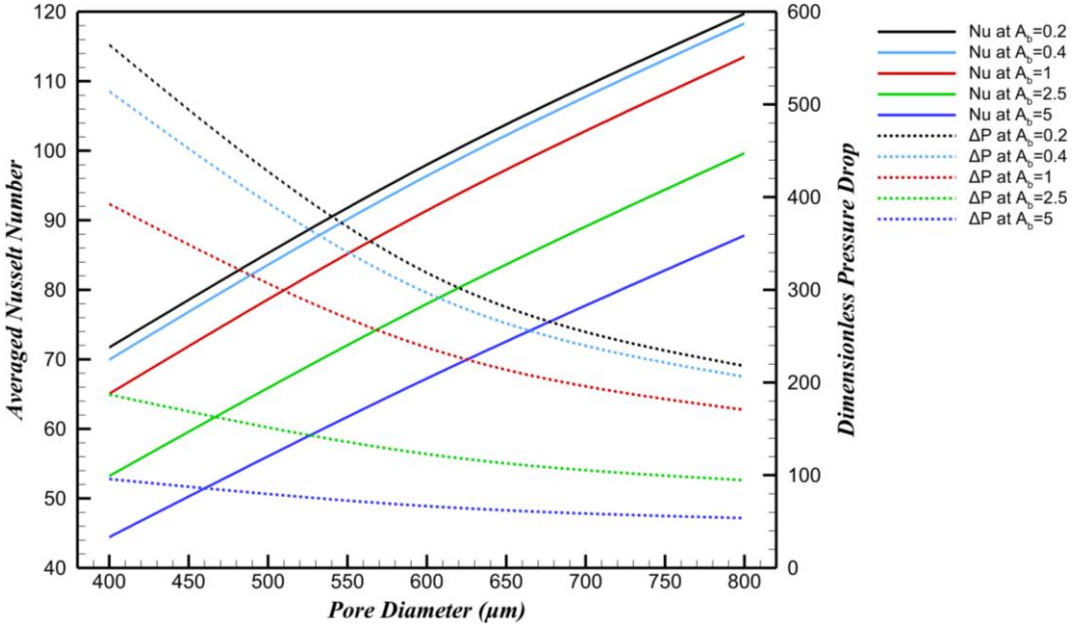

Fig. 9. Impact of pore size and baffles arrangement for FC-3283-cooled heat sinks.

This outcome becomes even more interesting when taking into account the significant amount of pressure drop saved, which is of economic priority in the design of high-power-density electronics. It is also noticed that while altering the arrangement of foam baffles, increasing the pore size results in an almost identical extent of improvement in the heat dissipation performance unlike the scenario found for pressure loss, which becomes less sensitive to pore

size variation at higher A_b ratios. This may be attributed to the reduction in the amount of coolant flowing through the foam structures as the A_b ratio increases.

The impact of porosity change along with the heat sink configuration on the performance attained can be summarized in Figs. 10 & 11 regarding the averaged Nusselt number and dimensionless pressure drop for $(D = 400\mu m)$ heat sinks cooled with a $\left(Re_{D_{in}} = 100\right)$ coolant stream and subjected to 5 and $50\,W/cm^2$ heat density for those cooled with air and FC-3283, respectively. As the heat dissipation capability, in general, deteriorates with the increase of foam porosity due to the reduction in the effective thermal conductivity and specific interstitial heat transfer area of the foam; there is, however, a noticeable saving in pressure drop, which is of great benefit in practice, particularly for those systems subjected to mild levels of heating. While changing the heat sink configuration, it is also observed that the increase in porosity influences the heat transfer performance almost identically unlike the response of pressure drop, which becomes less sensitive to porosity change in the in-parallel configured baffles heat sinks. This is due to the reduction in the airflow fraction penetrating through the porous structures when the baffles length-to-width ratio is increased.

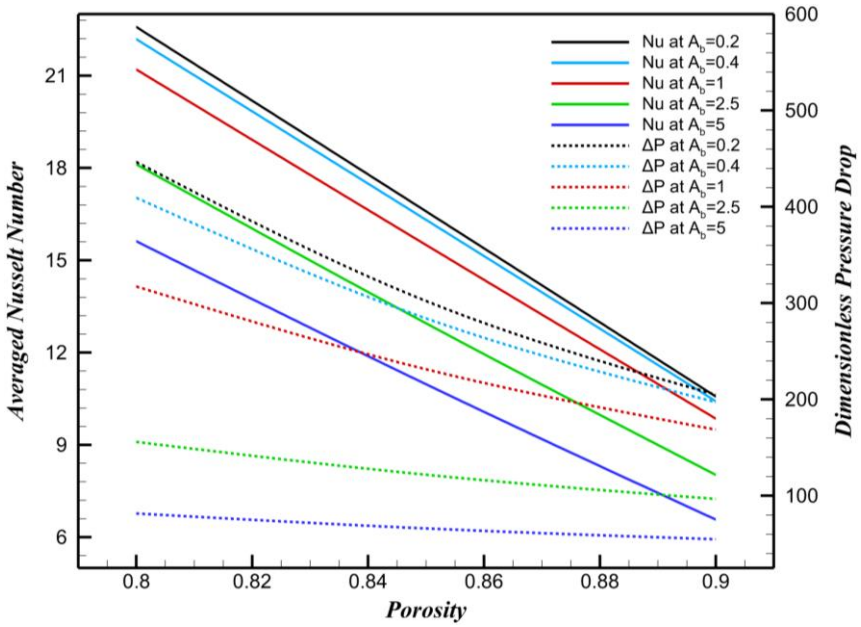

Fig. 10. Impact of porosity and baffles arrangement for air-cooled heat sinks.

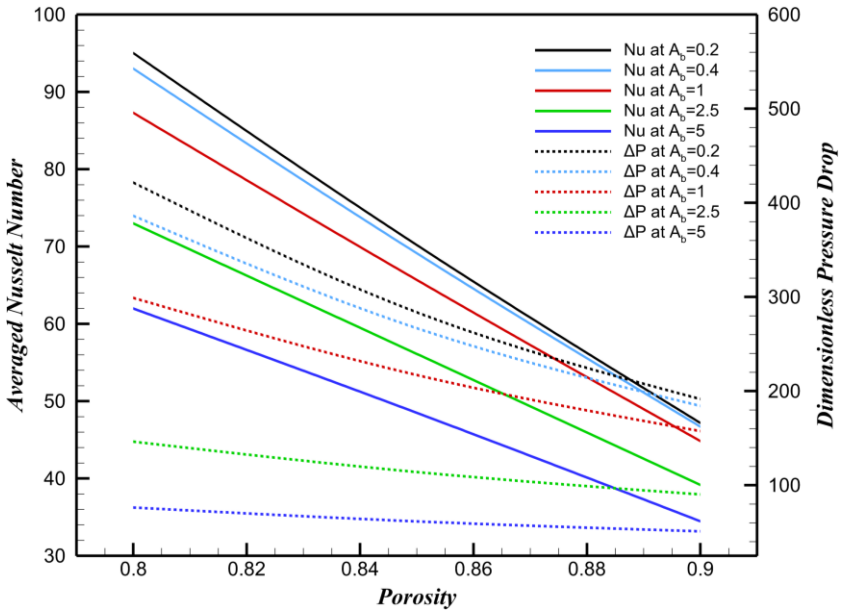

Fig. 11. Impact of porosity and baffles arrangement for FC-3283-cooled heat sinks.

4.3. Impact of operating conditions

As the current analysis is mainly focused on the design of graphite foam heat sinks capable to operate under heavy duties, it is essential to investigate the role played by operating conditions, under which the heat sinks proposed can perform efficiently. Those conditions are the pore-Reynolds number Re_D at the inlet boundary and the heat flux applied q_w on the heating surface. A balanced combination of these two parameters along with proper design conditions is most likely to result in safe operation with affordable pressure losses. Figs. 12 & 13 demonstrate the maximum temperature rise $\Delta T_{w\max}$ detected on the heated surface for a particular design and operating conditions of air- and FC-3283-cooled heat sinks, respectively. In general, heat sinks can respond sufficiently to the thermal loads applied as long as being cooled with a strong enough coolant stream. As preceded, the heat sinks with foam baffles aligned in perpendicular to the coolant mainstream outperform those with in-parallel aligned baffles for the corresponding operating conditions, where the maximum temperature $T_{w\max}$ rises remarkably while increasing the A_b ratio.

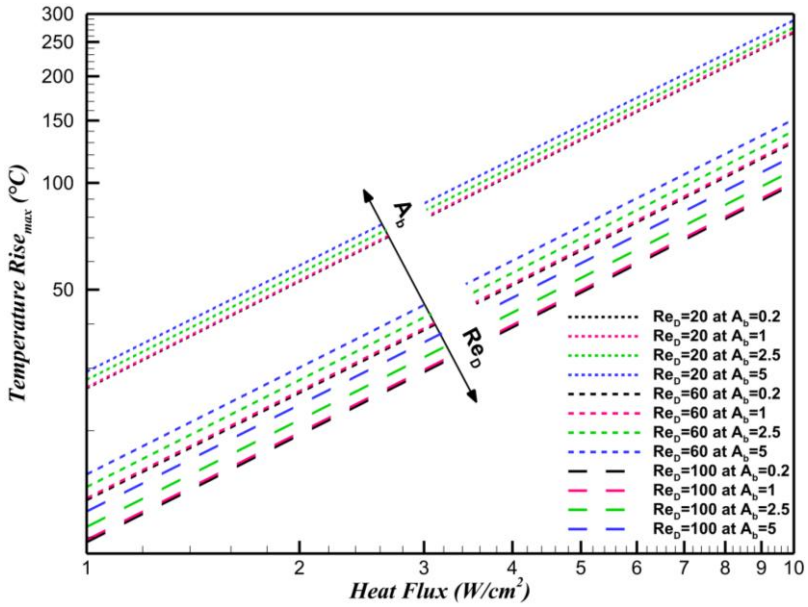

Fig. 12. Maximum temperature rise of ($\emptyset = 0.8$ & $D = 400\mu m$) air-cooled heat sinks.

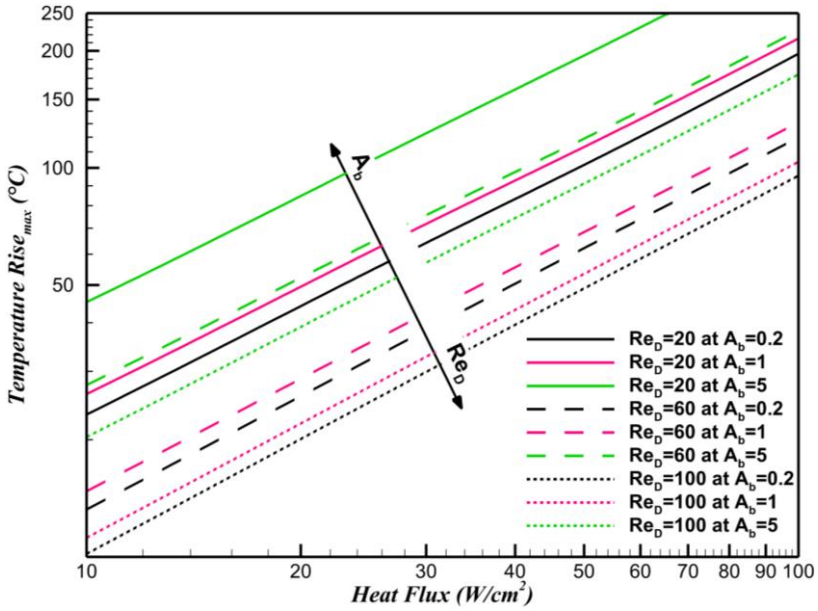

Fig. 13. Maximum temperature rise of ($\emptyset = 0.8$ & $D = 400\mu m$) FC-3283-cooled heat sinks.

To emphasis how outperforming the suggested heat sinks are, they have been compared with traditional air- and water-cooled techniques (Çengel and Ghajar, 2015) in terms of the maximum temperature rise $\Delta T_{w\max}$ monitored on the baseplate "for a wide range of heat densities imposed", as shown in Fig. 14. The currently suggested heat sinks are, in general, capable to get rid of hot spots effectively, where the maximum temperature rise monitored for a particular thermal load is approximately one-order of magnitude less than it is for the corresponding traditional cooling ways (Çengel and Ghajar, 2015). It is further worth mentioning that heat sinks formed of ($D = 400\mu m$ & $\emptyset = 0.8$) foam are the only enclosed within the design envelope illustrated. Thus, heat dissipation performance is anticipated to

either improve or deteriorate with the increase of foam pore diameter or porosity, respectively, but still outstanding.

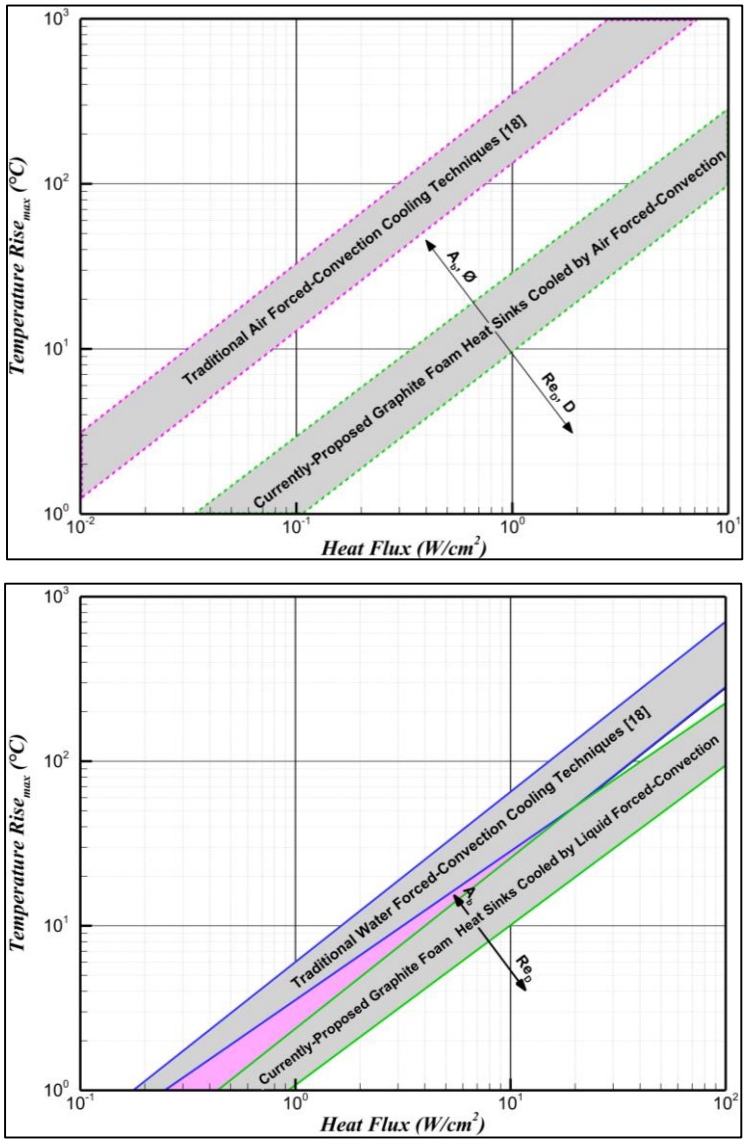

Fig. 14. Maximum temperature rise computed compared to traditional cooling techniques (Çengel and Ghajar, 2015) for air-cooled (up) and FC-3283 heat sinks.

4.4. Thermohydraulic performance

The effectiveness of a heat transfer enhancement technique can, in general, be evaluated using what known as the Thermal Performance Factor. It represents the ratio of the relative enhancement gained in heat transfer rate to the increase in friction factor due to the presence of the graphite foam heat sinks proposed. Hence, it can be defined as follows:

$$\eta = \frac{Nu/Nu_0}{(f/f_0)^{1/3}} = \frac{Nu/Nu_0}{(\Delta P/\Delta P_0)^{1/3}} \quad (6)$$

However, the above formulation does not reflect the desire to avoid the emergence of local spots heated excessively. Therefore, it is favourable to adopt a modified form that takes into consideration this crucial criterion while designing heat sinks for electronic cooling applications, as follows:

$$\eta_{\text{mod.}} = \eta \left(\frac{\Delta T_{w\max}}{\Delta T_{\text{allowed}}}\right)^{-1} = \left(\frac{Nu/Nu_0}{(\Delta P/\Delta P_0)^{1/3}}\right)/\left(\frac{T_{w\max}-T_{in}}{\Delta T_{\text{allowed}}}\right) \quad (7)$$

Where $T_{w\max}$ stands for maximum temperature detected on the heated surface, while $\Delta T_{\text{allowed}}$ is the maximum temperature rise allowed while operation. Assuming that the maximum temperature allowed $T_{w\max}$ is limited to $125℃$, as recommended for junction temperatures in silicon-based semiconductor devices (Çengel and Ghajar, 2015), then the maximum temperature rise considered here will be $\Delta T_{\text{allowed}} = 100℃$. So, as long as the modified thermal performance factor $(\eta_{\text{mod.}})$ is higher than or equal to the traditional one (η), the designed system runs under safe operating conditions, where no undesirable hot spots are found.

Fig. 15 summarizes the performance achieved using the heat sinks configurations proposed for various pore diameters. The air-cooled heat sinks are subjected to $(q_w = 5\,W/cm^2)$ heat density, while the corresponding FC-3283-cooled ones are exposed to one-order higher thermal load, i.e. $q_w = 50\,W/cm^2$. The system performance, in general, improves while increasing the pore size due to the enhancement acquired in heat transfer accompanied by significant saving in pressure drop. At first glance, it is apparent that the overall performance improves with increase in the (A_b) ratio. However, the modified form of thermal performance factor $\eta_{\text{mod.}}$ exhibits a different trend, where $(A_b = 1)$ air-cooled heat sinks outperform with the increase of pore size unlike the $(A_b = 5)$ ones that become less efficient, while the FC-3283-cooled heat sinks formed of perpendicular-to-flow baffles outperform those formed of parallel-to-flow baffles. This is due to the differences in response to the thermal load applied, where the heat sink configured of in-parallel aligned baffles responds modestly to the heat flux imposed although it causes no excessive losses in pressure as it is the case with the heat sink formed of baffles aligned perpendicularly to the coolant mainstream.

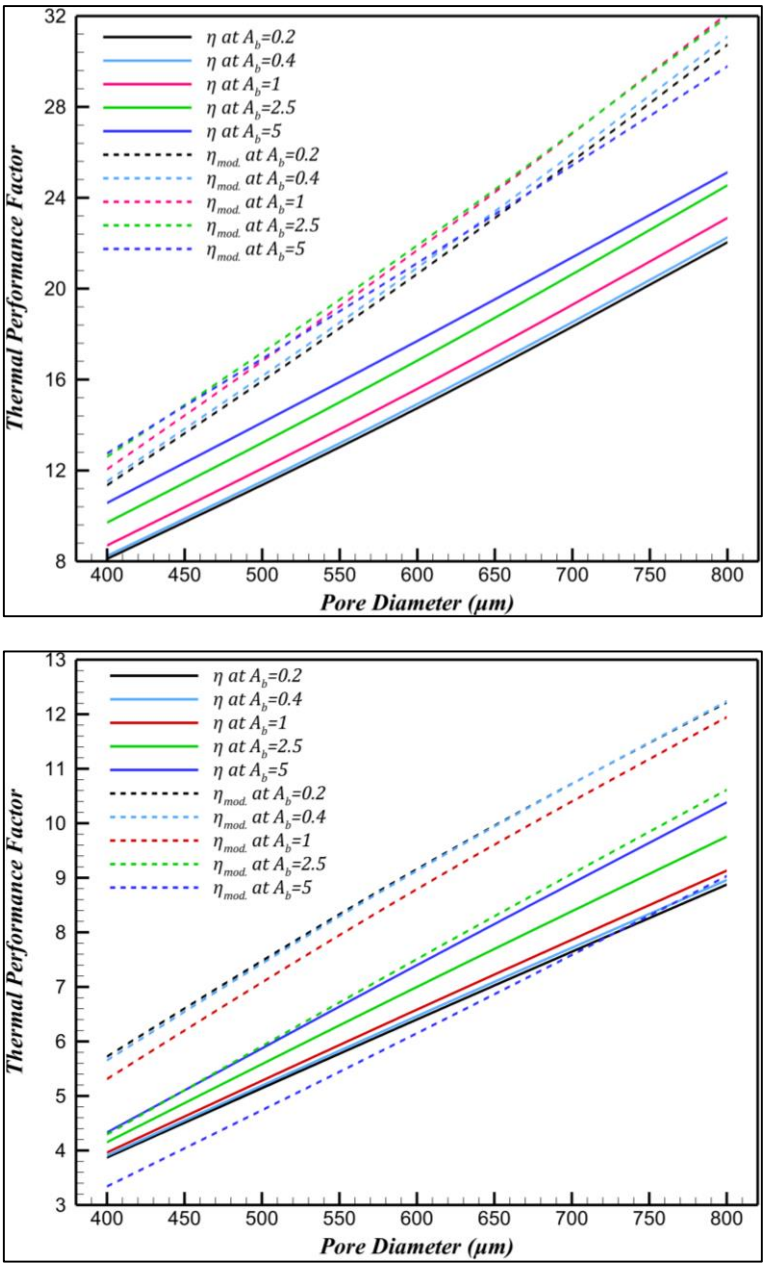

Fig. 15. Thermal performance factor and its modified form with pore size and configuration of air-cooled (up) and FC-3283-cooled (down) heat sinks for $Re_{p_{in}} = 100$.

The effect of foam porosity in combination with the heat sink configuration on the overall performance is illustrated in Fig. 16. In general, the performance factor deteriorates while increasing the foam porosity due to the reduction in the heat sink ability to dissipate heat effectively despite the saving acquired in pressure drop. It is also observed that heat sinks with higher (A_b) ratios have, in general, better η values due to the slight drop recorded in pressure regardless of their relatively poor ability to dissipate heat. Based on the modified form of thermo-hydraulic performance factor $(\eta_{\text{mod.}})$, which gives a more realistic insight into the gross performance attained, heat sinks with higher (A_b) ratios exhibit a worse performance than other

configurations due to their poor capability to dissipate heat sufficiently, which in turn allows hot spots to arise on the chip surface.

Overall, heat sinks with $(A_b = 0.2)$ configuration and formed of foam with low porosity and large pores, i.e. $\emptyset = 0.8$ & $D = 800\mu m$, mostly exhibit the best performance to be fulfilled in high-performance electronics as they are capable to dissipate extreme heat generated there regardless of the relatively high-pressure drop resulted.

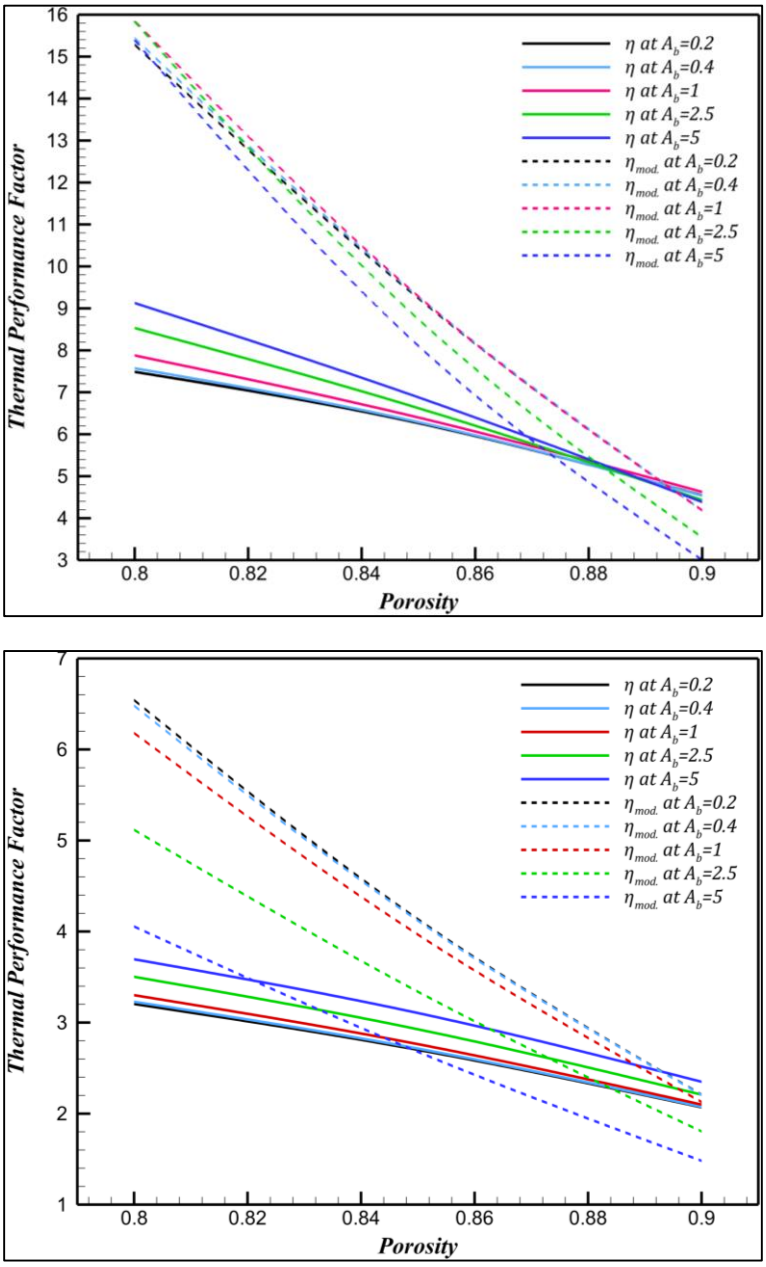

Fig. 16. Thermal performance factor and its modified form with pore size and configuration of air-cooled (up) and FC-3283-cooled (down) heat sinks for $Re_{p_{in}} = 100$.

5. CONCLUSIONS

Highly-conductive graphite foam has been used to effectively dissipate the heat generated in electronic components. The air- and FC-3283-cooled heat sinks suggested have been configured from staggered foamed-baffles arranged either in parallel or perpendicular to the coolant paths through the slots in between to reduce the pressure drop. The performance of the currently proposed heat sinks has been examined numerically using the Simcenter STAR-CCM+ CFD commercial code. A wide range of design parameters have been tested including the heat sink configuration along with structural characteristics of the graphite foam used. It has been found that foam baffles oriented perpendicular to the path of coolant flow can dissipate heat by about 50% better than those parallel to it, but with higher pressure losses. It has also been found that heat dissipation capability, for a certain orientation of baffles, can be improved by up to 100% when the foam pore size is doubled with outstanding saving in pressure losses by up to 300%. The impact of operating conditions, including the inlet coolant flowrate and heat flux applied, has also been inspected. The results computed indicate that heat sink capability to dissipate heat can be improved either with increasing the foam pore size or decreasing the foam porosity and/or the (A_b) ratio. Significant amount of pressure drop can, on the other hand, be saved while increasing any of the foam porosity, pore diameter, or (A_b) ratio. The currently proposed heat sinks have been found efficient to meet the extremely thermal demands of high-performance electronic equipment and sweep away the heat generated there with a reasonable cost of pressure drop, where hot spots can be eliminated with proper manipulation of design conditions. Extreme operating conditions, i.e. with heat density of up to 10W/cm^2 for air-cooled heat sinks and 100W/cm^2 for those cooled with FC-3283, can be well managed when a heat sink is configured from baffles that are oriented perpendicularly to the coolant flow path and formed of graphite foam having low porosity ($\emptyset = 0.8$) and larger pore size ($D = 800\mu m$).

6. REFERANCES

3MTM (2019) 3MTM FluorinertTM Electronic Liquid FC-3283 Technical Data Sheet. St. Paul, Minnesota, USA.

Al-Aabidy, Q., Alhusseny, A. and Al-Zurfi, N. (2021) ‘Numerical investigation of turbulent flow in a wavy channel partially filled with a porous layer’, International Journal of Heat and Mass Transfer, 174, p. 121327.

Alhusseny, A., Turan, A., Nasser, A., & Hidri, F. (2015). Hydrodynamically and thermally developing flow in a rectangular channel filled with a high porosity fiber and rotating about a parallel axis. International Communications in Heat and Mass Transfer, 67, 114-123.

Alhusseny, A., Al-Zurfi, N., Nasser, A., Al-Fatlawi, A., & Aljanabi, M. (2020). Impact of using a PCM-metal foam composite on charging/discharging process of bundled-tube LHTES units. International Journal of Heat and Mass Transfer, 150, 119320.

Alhusseny, A., Al-Aabidy, Q., Al-Zurfi, N., Nasser, A., & Aljanabi, M. (2021). Cooling of high-performance electronic equipment using graphite foam heat sinks. Applied Thermal Engineering, 191, 116844.

Alhusseny, A., Al-Fatlawi, A., Al-Aabidy, Q., Nasser, A., & Al-Zurfi, N. (2021). Dissipating the heat generated in high-performance electronics using graphitic foam heat-sinks cooled with a dielectric liquid. International Communications in Heat and Mass Transfer, 127, 105478.

Alhusseny, A., Turan, A., & Nasser, A. (2017). Rotating metal foam structures for performance enhancement of double-pipe heat exchangers. International Journal of Heat and Mass Transfer, 105, 124-139.

Çengel, Y. A. and Ghajar, A. J. (2015) Heat and Mass Transfer: Fundamentals & Applications. 5th edn. New York, USA: McGraw-Hill Education.

DeGroot, C. T. and Straatman, A. G. (2012) 'Numerical results for the effective flow and thermal properties of idealized graphite foam', Journal of Heat Transfer, 134, pp. 042603-1–12.

Gallego, N. C. and Klett, J. W. (2003) 'Carbon foams for thermal management', Carbon, 41, pp. 1461–1466.

Klett, J., Hardy, R., Romine, E., Walls, C., & Burchell, T. (2000). High-thermal-conductivity, mesophase-pitch-derived carbon foams: effect of precursor on structure and properties. Carbon, 38(7), 953-973.

Klett, J., Ott, R. and McMillan, A. (2000) 'Heat exchangers for heavy vehicles utilizing high thermal conductivity graphite foams', SAE Technical Paper, 2000-01–22.

Leong, K. C., Li, H. Y., Jin, L. W., & Chai, J. C. (2010). Numerical and experimental study of forced convection in graphite foams of different configurations. Applied Thermal Engineering, 30(5), 520-532.

Lin, W., Sundén, B. and Yuan, J. (2013) 'A performance analysis of porous graphite foam heat exchangers in vehicles', Applied Thermal Engineering. Elsevier Ltd, 50(1), pp. 1201–1210.

Lin, W., Yuan, J. and Sunden, B. (2011) 'Review on Graphite Foam as Thermal Material for Heat Exchangers', in World Renewable Energy Congress 2011. Linköping, Sweden: Energy End-Use Efficiency Issues (EEE).

Lin, Y. R. et al. (2010) 'Experimental study on heat transfer and pressure drop of recuperative heat exchangers using carbon foam', Journal of Heat Transfer, 132(9), pp. 091902-1–10.

Ochoa-Tapia, J. A. and Whitaker, S. (1997) 'Heat transfer at the boundary between a porous medium and a homogeneous fluid', International Journal of Heat and Mass Transfer, 40(11), pp. 2691–2707. doi: 10.1615/JPorMedia.v1.i1.30.

Ott, R. D., Zaltash, A. and Klett, J. W. (2002) 'Utilization of a graphite foam radiator on a natural gas engine-driven heat pump', in ASME 2002 International Mechanical Engineering Congress and Exposition. New Orleans, USA: ASME.

Qu, J. G. et al. (2024) 'Experimental study on heat transfer during melting in metal and carbon foam saturated with phase-change materials for temperature control in electronic devices', 236, p. 121681. doi: 10.1016/j.applthermaleng.2023.121681.

Straatman, A. G. et al. (2007) 'Characterization of porous carbon foam as a material for compact recuperators', Journal of Engineering for Gas Turbines and Power, 129, pp. 326–330. doi: 10.1115/1.2436562.

Straatman, A. G. (2011) 'Heat Transfer in Graphitic Foams', in O¨chsner, A. and Murch, G. E. (eds) Heat Transfer in Multi-Phase Materials. Springer-Verlag Berlin Heidelberg, pp. 101–129. doi: 10.1007/8611.

Thompson, B. E. (2014) 'Heat transfer in porous graphite foams', Journal of Heat Transfer, 136(3), pp. 032602-1–7. doi: 10.1115/1.4025905.

Wu, W., Du, J. H., Lin, Y. R., Chow, L. C., & Notardonato, W. (2009). Design and experiment of compact and effective carbon foam recuperative heat exchangers. Journal of thermophysics and heat transfer, 23(2), 339-345.

Yu, Q., Thompson, B. E. and Straatman, A. G. (2006) 'A unit cube-based model for heat transfer and fluid flow in porous carbon foam', Journal of Heat Transfer, 128, pp. 352–360. doi: 10.1115/1.2165203.